

## Electronic Supplementary Information File of the paper

# Chemical selectivity in structure determination by time dependent analysis of in situ XRPD data: a clear view of Xe thermal behavior inside a MFI zeolite

by

Luca Palin,<sup>a,b</sup> Rocco Caliendo,<sup>c</sup> Davide Viterbo,<sup>a</sup> Marco Milanese<sup>a,\*</sup>

*a* Dipartimento di Scienze e Innovazione Tecnologica, Università del Piemonte Orientale "A. Avogadro" (Italy), Via Michel 11, I-15121 Alessandria, Italy. E-mail: marco.milanesio@uniupo.it

*b* Nova Res s.r.l., Via Dolores Bello 3, 28100 Novara, Italy (<http://www.novares.org>)

*c* Institute of Crystallography, CNR, via Amendola 122/o, Bari 70126, Italy.

### Section 1: The MED theory for powder data

The MED equation for modulation of occupancy factor have been reported in a previous paper [Caliandro, R., H., Chernyshov, D., Emerich, H., Milanese, M., Palin, L., Urakawa, A., van Beek, W., Viterbo, D., 2012, *J. Appl. Cryst.*, 45, 458-470.]. Here we treat the case of X-ray powder diffraction. Suppose we collect a set of powder diffraction patterns by periodically changing an external parameter using an external stimulus. Each measured pattern may be described by the following function:

$$A(2\vartheta, t) = \sum_{\mathbf{Q}} m_{\mathbf{Q}} L_{\mathbf{Q}} |F_{\mathbf{Q}}|^2 f(2\vartheta, 2\vartheta_{\mathbf{Q}}) - b(2\vartheta) \quad (\text{SI-1})$$

where  $m_{\mathbf{Q}}$  is the multiplicity of the reflection  $\mathbf{Q} = \mathbf{Q}_{HKL}$  (here we assume that this quantity is not varying with time),  $L_{\mathbf{Q}}$  is the Lorentz-Polarization factor,  $f(2\vartheta, 2\vartheta_{\mathbf{Q}})$  is a function describing the peak centred at  $2\vartheta_{\mathbf{Q}}$  (typically a Gaussian or Lorentian shape) and  $b(2\vartheta)$  is the function describing the background.

We apply the demodulation procedure to the set of measured patterns according to the simplest decomposition integral, following a scheme identical to the one used in spectroscopy (Urakawa *et al.*, 2006):

$$A_k(2\vartheta, \phi) = \frac{2}{t_p} \int_0^{t_p} A(2\vartheta, t) \sin(k\Omega t + \phi) dt \quad (\text{SI-2})$$

If the background contribution and the peak shape function does not change with time (a reasonable assumption if crystallite size and defectivity are not affected by the stimulus), eq. (SI-2) is arranged as:

$$A_k(2\vartheta, \phi) = \sum_{\mathbf{Q}} m_{\mathbf{Q}} L_{\mathbf{Q}} f(2\vartheta, 2\vartheta_{\mathbf{Q}}) \frac{2}{t_p} \int_0^{t_p} |F_{\mathbf{Q}}|^2 \sin(k\Omega t + \phi) dt \quad (\text{SI-3})$$

Hereafter, we only consider the following time-dependent quantity.

$$A_k(\mathbf{Q}, \phi) = \frac{2}{t_p} \int_0^{t_p} |F_{\mathbf{Q}}|^2 \sin(k\Omega t + \phi) dt \quad (\text{SI-4})$$

Let us assume that only one sub-set of atoms in a multi-atomic structure is responding to the external perturbation, so that

$$|F_{\mathbf{Q}}|^2 = |F_A(t) + F_S|^2 = |F_A(t)|^2 + |F_S|^2 + F_A(t)F_S^* + F_A^*(t)F_S \quad (\text{SI-5})$$

where A and S stand for actively responding and spectator sub-lattices, respectively. The decomposition integral (SI-4) applied to eq. (SI-5) extracts only the time-dependent terms and suppresses the time-independent contribution arising from  $|F_S|^2$ , leading to:

$$A_k(\mathbf{Q}, \phi) = \frac{2}{t_p} \int_0^{t_p} |F_A|^2 \sin(k\Omega t + \phi) dt + \frac{2}{t_p} \int_0^{t_p} [F_A(t)F_S^* + F_A^*(t)F_S] \sin(k\Omega t + \phi) dt \quad (\text{SI-6})$$

Let us now suppose that the crystal responds to the external stimulus by changing in time the occupancy of some “active” atoms, according to the following function:

$$\mu_i(t) = a + b \sin(\Omega t + \varphi). \quad (\text{SI-7})$$

where a and b ensure that the occupancy varies from 0 to 1 and  $\varphi$  represents the delay of the response with respect to the stimulus.

In this case the structure factor for the active atoms may be written:

$$F_A(t) = \sum_i^A [a + b \sin(\Omega t + \varphi)] f_i \exp(i\mathbf{Q}\mathbf{R}_i)$$

where  $f_i$ ,  $\mathbf{R}_i$ ,  $\mu_i$  indicate respectively the scattering factor for X-rays, the position vector and the occupancy for corresponding atom. Eq. (6) then becomes:

$$\begin{aligned} A_k(\mathbf{Q}, \phi) = & \frac{2}{t_p} \int_0^{t_p} |a + b \sin(\Omega t + \varphi)|^2 \sin(k\Omega t + \phi) dt \left| \sum_i^A f_i \exp(i\mathbf{Q}\mathbf{R}_i) \right|^2 + \\ & + \frac{2}{t_p} \int_0^{t_p} |a + b \sin(\Omega t + \varphi)| \sin(k\Omega t + \phi) dt \left\{ F_S^* \sum_i^A f_i \exp(i\mathbf{Q}\mathbf{R}_i) + F_S \sum_i^A f_i \exp(-i\mathbf{Q}\mathbf{R}_i) \right\} \end{aligned} \quad (\text{SI-8})$$

The phase-sensitive detection carried out at different demodulation indices  $k$  gives:

- 1)  $k=1$ :

$$\begin{cases} \frac{2}{t_p} \int_0^{t_p} |a + b \sin(\Omega t + \varphi)|^2 \sin(\Omega t + \varphi) dt = 2ab \cos(\varphi - \phi) \\ \frac{2}{t_p} \int_0^{t_p} |a + b \sin(\Omega t + \varphi)| \sin(\Omega t + \varphi) dt = b \cos(\varphi - \phi) \end{cases} \quad (\text{SI-9})$$

Therefore, eq. (SI-8) may be written as:

$$A_1(\mathbf{Q}, \phi) = 2b \cos(\varphi - \phi) \left[ a \left| \sum_i^A \mu_{i0} f_i \exp(i\mathbf{QR}_i) \right|^2 + F_S^* \sum_i^A \mu_{i0} f_i \exp(i\mathbf{QR}_i) + F_S \sum_i^A \mu_{i0} f_i \exp(-i\mathbf{QR}_i) \right]$$

2)  $k=2$ :

$$\begin{cases} \frac{2}{t_p} \int_0^{t_p} |a + b \sin(\Omega t + \varphi)|^2 \sin(2\Omega t + \phi) dt = \frac{b^2}{2} \sin(2\varphi - \phi) \\ \frac{2}{t_p} \int_0^{t_p} |a + b \sin(\Omega t + \varphi)| \sin(2\Omega t + \phi) dt = 0 \end{cases} \quad (\text{SI-10})$$

Therefore, eq. (SI-8) may be written as:

$$A_2(\mathbf{Q}, \phi) = \frac{b^2 \sin(2\varphi - \phi)}{2} \left[ \left| \sum_i^A \mu_{i0} f_i \exp(i\mathbf{QR}_i) \right|^2 \right]$$

3)  $k>2$ :

$$\begin{cases} \frac{2}{t_p} \int_0^{t_p} |a + b \sin(\Omega t + \varphi)|^2 \sin(2\Omega t + \phi) dt = 0 \\ \frac{2}{t_p} \int_0^{t_p} |a + b \sin(\Omega t + \varphi)| \sin(2\Omega t + \phi) dt = 0 \end{cases} \quad (\text{SI-11})$$

Therefore, eq. (SI-8) may be written as:

$$A_3(\mathbf{Q}, \phi) = 0$$

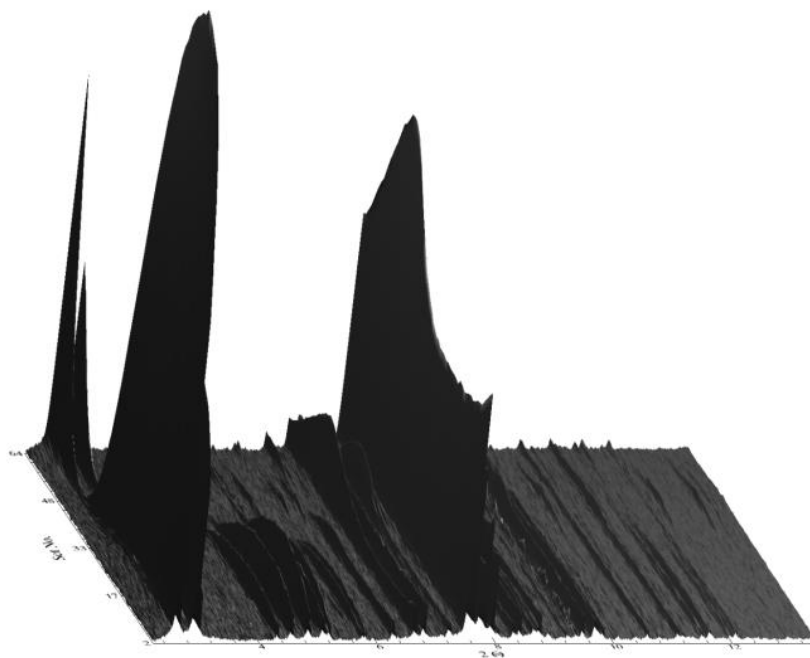
**The following conclusions may be drawn:**

- the demodulation at  $k=2$  has contribution only from active atoms;
- the demodulation at  $k=1$  has contributions from active atoms and from the mixed term active-spectator atoms;
- no demodulation signal is foreseen at higher harmonic frequencies higher than  $2\Omega$ ;
- the  $1\Omega$  demodulation is proportional to the the amplitude  $b$  of the occupancy variation, the  $2\Omega$  demodulation is proportional to the square of  $b$ ;

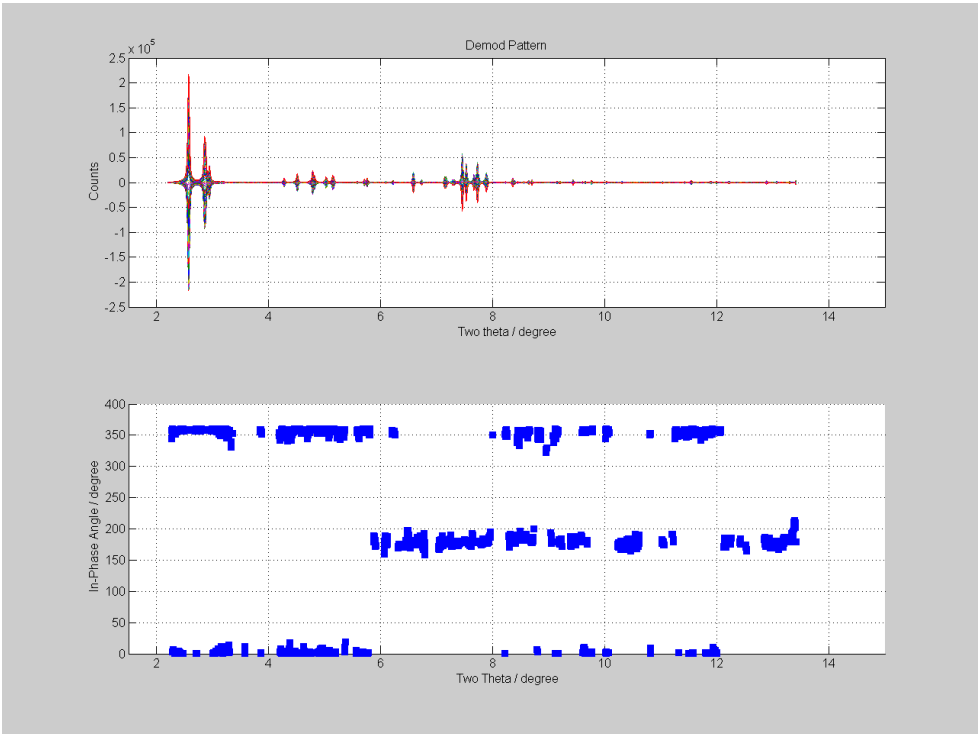
- the contribution from active atoms in the  $1\Omega$  demodulation is proportional to the average value  $a$  of the occupancy variations;
- the phase delay appears as a double quantity in  $2\Omega$  demodulation and as a single one in the  $1\Omega$  demodulation:
- the in-phase conditions for the  $1\Omega$  and  $2\Omega$  demodulated signals are respectively  $\varphi - \phi = 0^\circ$  and  $2\varphi - \phi = 270^\circ$ , corresponding to the occurrence of maximum values for the functions  $A_1(\mathbf{Q}, \phi)$  and  $A_2(\mathbf{Q}, \phi)$ .

The real experiments are measured very slow compared to the kinetics of the sorption process, so that the response is not delayed with respect to the stimulus ( $\varphi = 0^\circ$ ) and the in-phase angles are thus expected to be  $\phi = 0^\circ$  and  $\phi = 270^\circ$  for respectively  $1\Omega$  and  $2\Omega$  demodulated spectra. The present approach does not take into account lattice variation occurring during the experiment, and their importance will be discussed in the real experiment description (section 3.2.1 of the main paper and section 3 of the present ESI file)

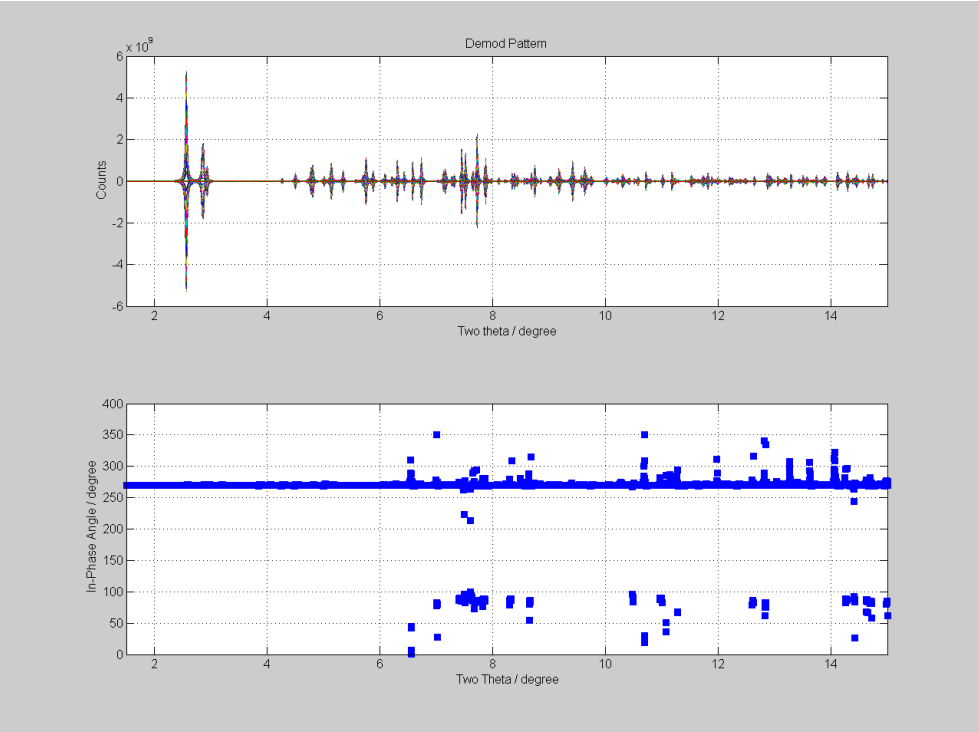
## Section 2 – Simulated and preliminary MED experiments



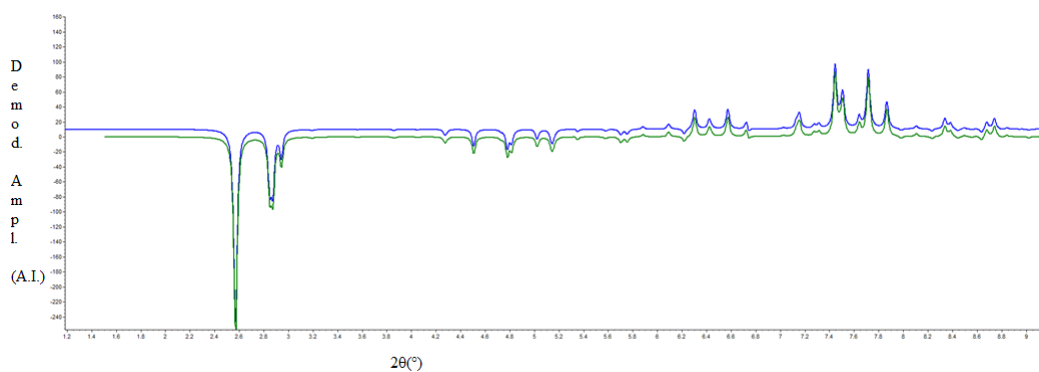
(a)



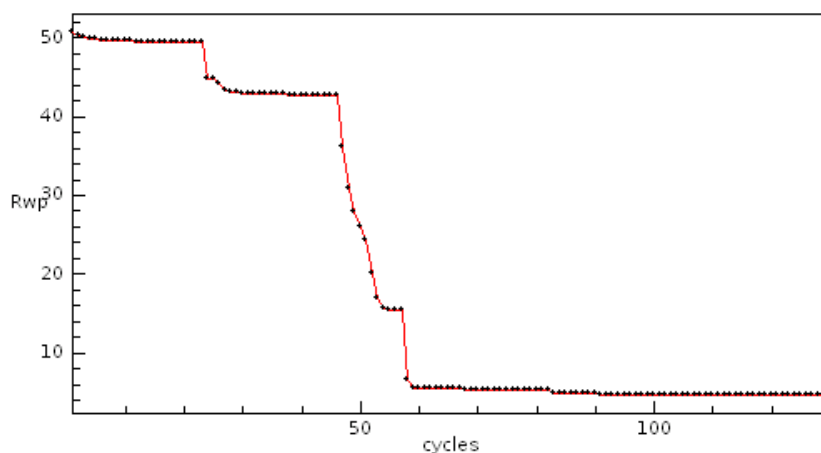
(b)



(c)



(d)



(e)

Figure SI-1: Demodulation at  $2\Omega$  on simulated data: (a) Simulated in situ XRPD data by a sinus modulation of Xe occupancy inside a MFI static framework; in-phase angle plot and demodulated pattern of  $1\Omega$  (b) and  $2\Omega$  (c) for the sinus stimulus simulation; (d) comparison of PC1 and  $2\Omega$  (blue) (green) scaled on the intensity of the largest peak to highlight the differences; (e) evolution of agreement factor during Xe substructure solution using the  $2\Omega$  demodulated pattern by the EXPO software.

### Section 3 - The large amplitude stimulus case (experiment T1 in Table 1 of the paper)

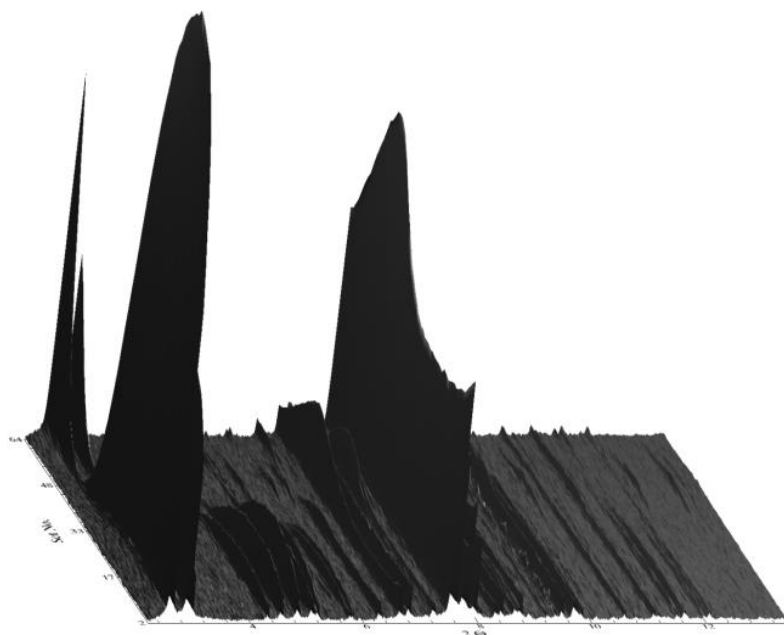
The collected XRPD data showed a modulation of peak intensity (Figure SI-2a) apparently not different from that shown by simulated data. However a qualitative comparison between the stimulus shape and the intensity trend revealed that the intensity varies with a sinusoidal-like trend, different from the triangular stimulus. This is an indication that the response is not the expected one, while, in the simulated experiment the intensity trend was identical to the stimulus trend. The in-phase angle analysis, reported in Figures S3 and S4 for the  $1\Omega$  and  $2\Omega$  decompositions respectively, shows a trend similar to the simulated one, with the same values of in-phase angles.

The corresponding  $2\Omega$  demodulated patterns exhibit negative peaks, which may be ascribed to:

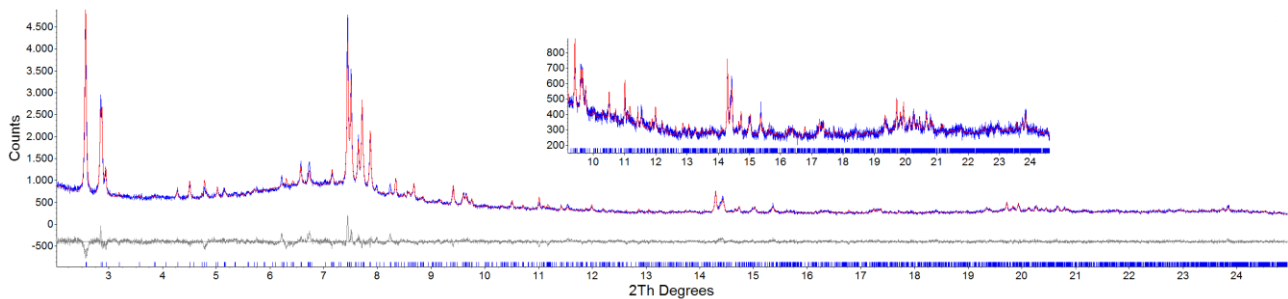
i) lattice variations during the experiment, which causes a drift of the peak positions in the powder profiles as a function of time. This effect cannot be taken into account in the pattern demodulation procedure;

ii) the non-linear response of the samples to the stimulus, i.e. violation of eq. 13 Si-8.

The pattern demodulated at  $2\Omega$  is reported in Figure SI-5, superimposed to that obtained from simulated data. The presence of negative peaks frustrated any attempt at obtaining a useful pattern for structure solution, due to the negative peaks and the difficulty to extract intensities of positive peaks from such powder peak profiles, hugely affected by lattice variation. Confirmation of non linear behavior is given by refined Xe occupancy from the T1 experiment, which does not follow the triangular shape of the stimulus (Figure SI-8). Moreover the behavior of the Xe atom in straight and sinusoidal channel is not identical, a further difference between simulated and experimental data. A linear response region is indeed found (see Figure SI-8) and a small amplitude stimulus in this region can be designed. Experiments T2, and T3 explored this linear region (red line in Figure SI-8).

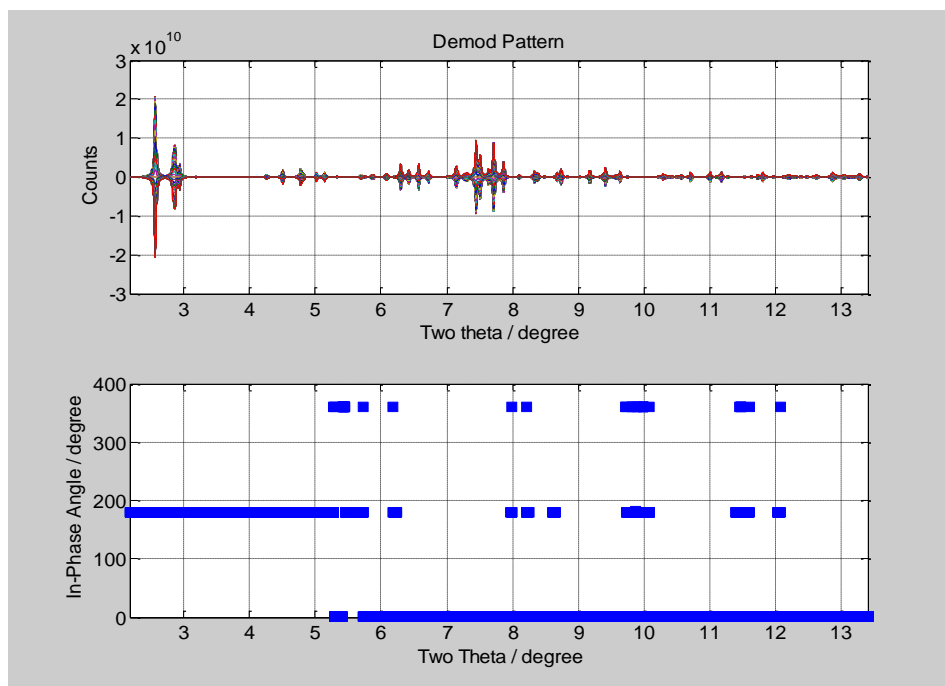


(a)

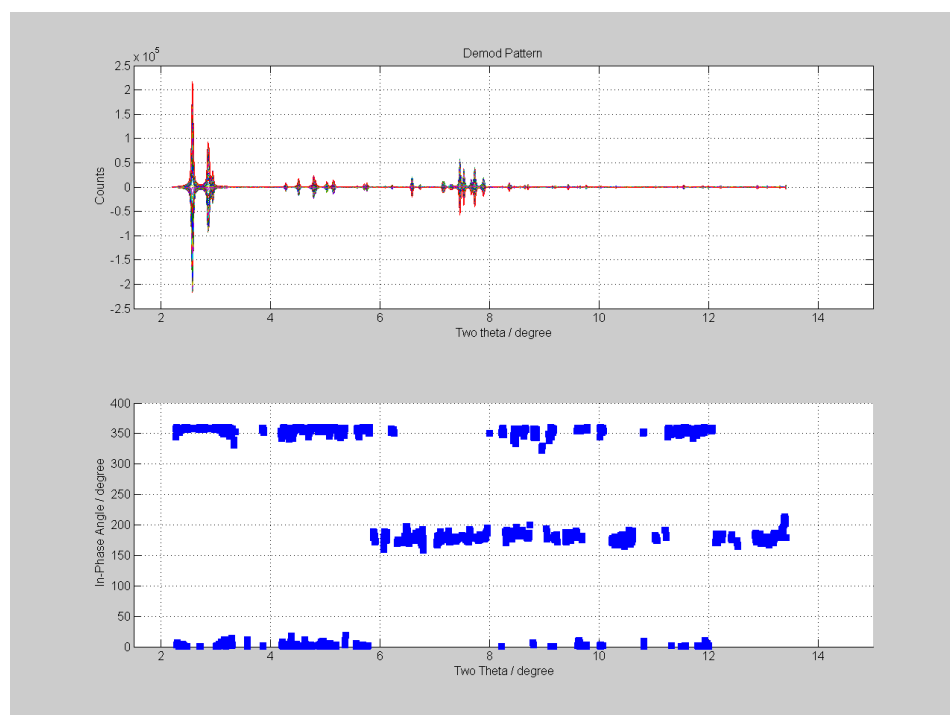


(b)

Figure SI-2: (a) Preliminary experimental MED data, dataset T1, by a large amplitude temperature triangular stimulus and (b) refinement by Topas TA of a static pattern, with 140 mbar of Xe at RT K.

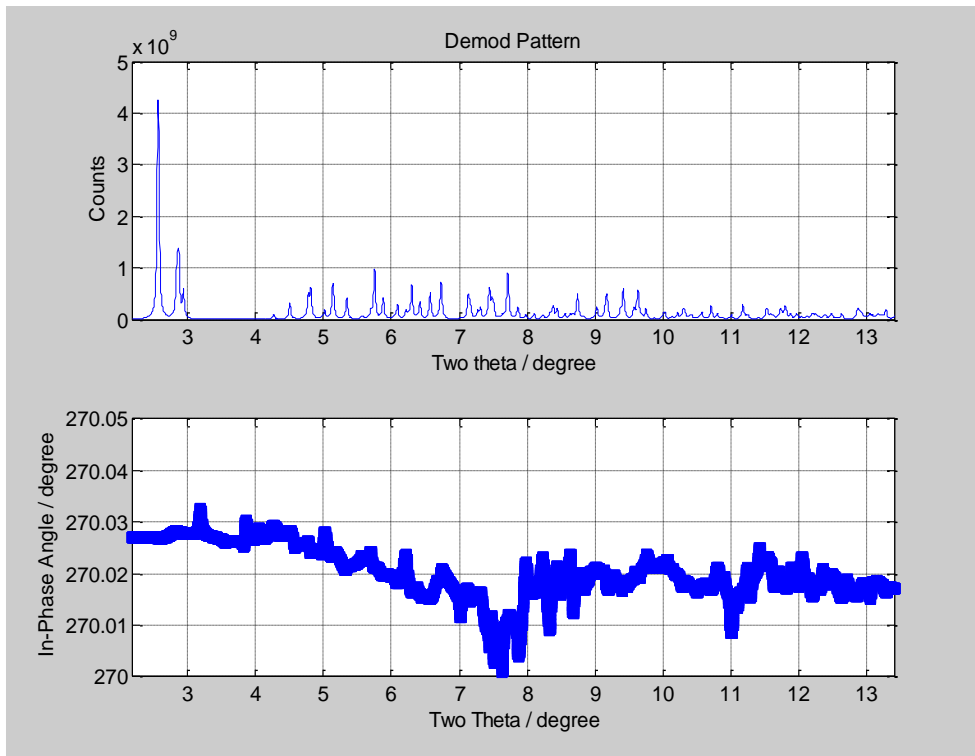


(a)

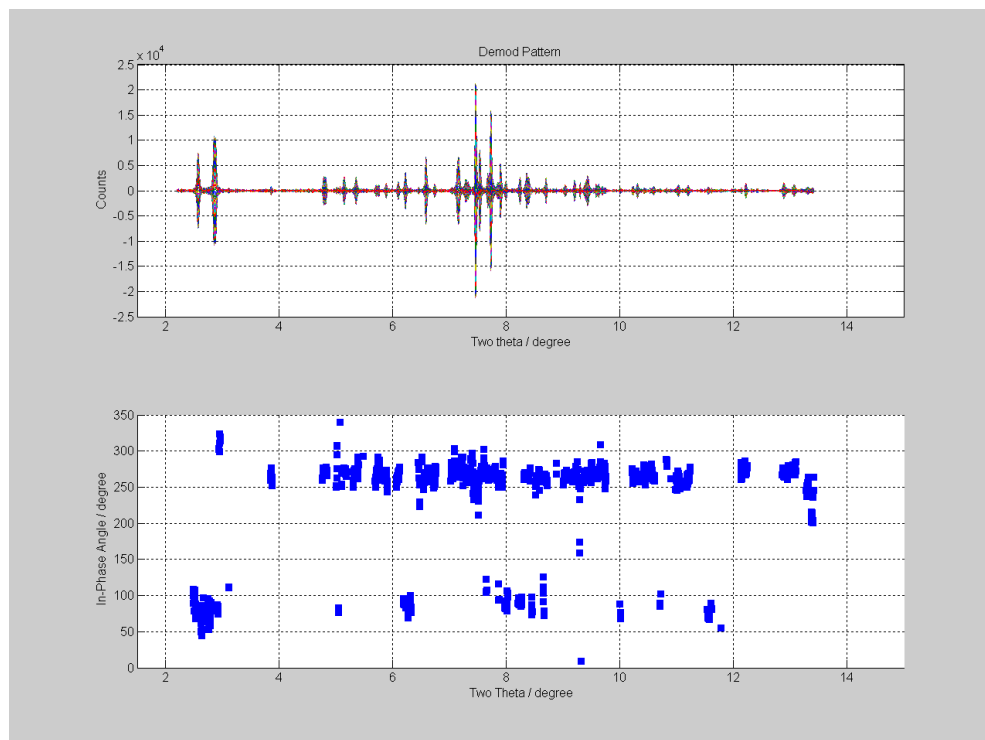


(b)

Figure SI-3: Results of the PSD at  $1\Omega$  on (a) simulated) and (b) real data by a triangle-shaped modulation: in (a) the occupancy was modulated in the simulation, in (b) the temperature was experimentally modulated.



(a)



(b)

Figure SI-4: Results of the PSD at  $2\Omega$  on (a) simulated and (b) real data by a triangle-shape stimulus; in (a) the occupancy was modulated in the simulation, in (b) the temperature was experimentally modulated.

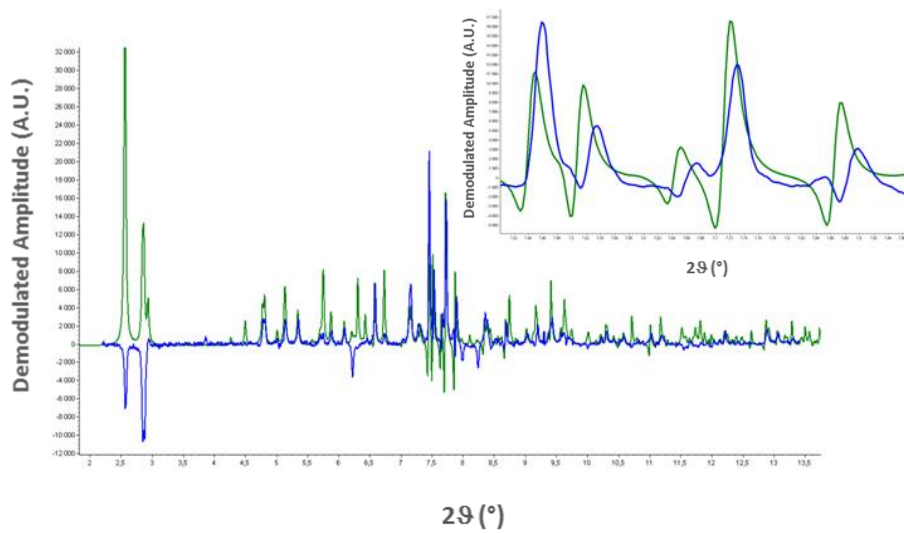


Figure SI-5: Simulated by a sinus stimulus (green) vs. experimental (blue)  $2\Omega$  demodulated pattern from the T1 experiment.

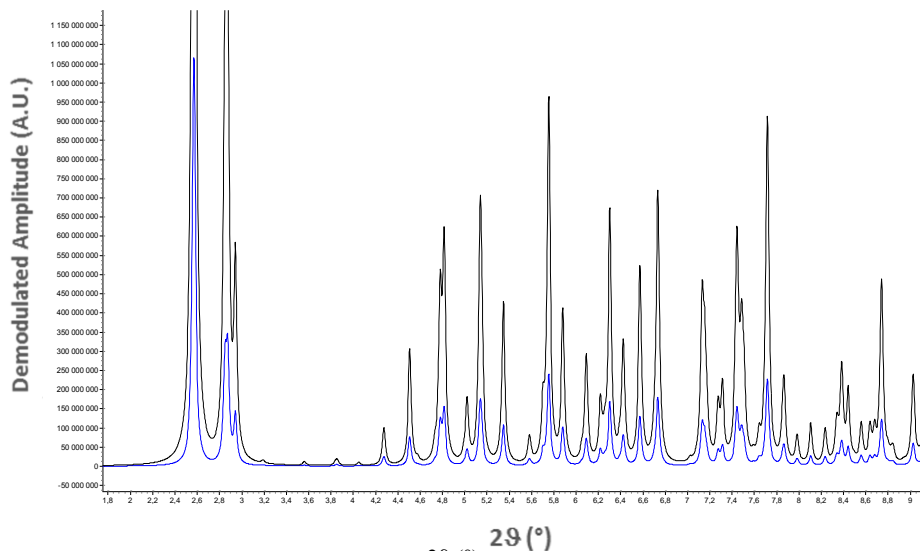


Figure SI-6 comparison of demodulated XRPD pattern with variation of occupancy (with a sinus shape) in the range 0-1 (Black curve) and 0.25-0.75 (blue curve) from simulated data: data are not scaled.

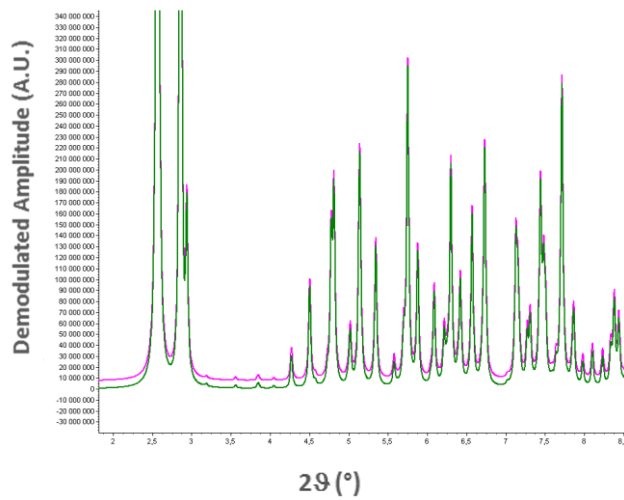


Figure SI-7: Same data as in figure SI-6, with large (green) and small (pink) occupancy variation, after scaling. No difference is observed in the simulated error-free data.

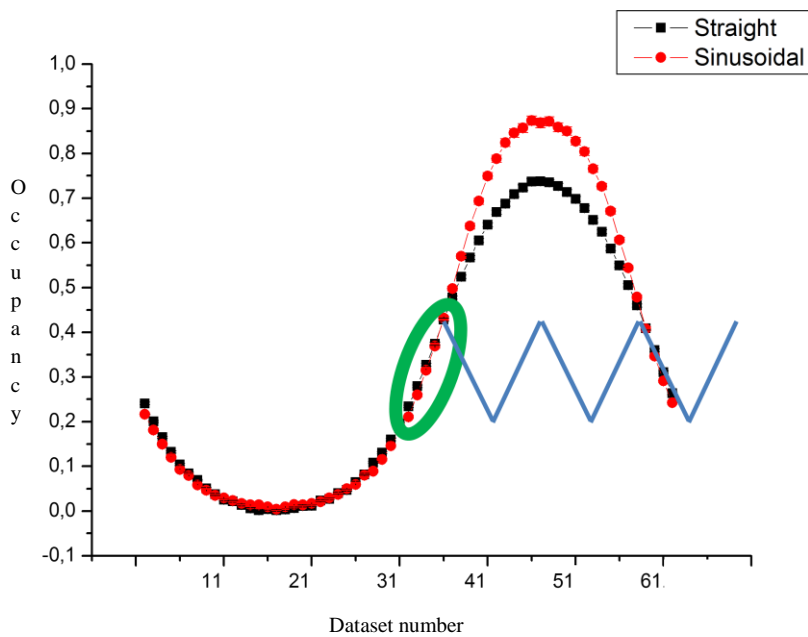
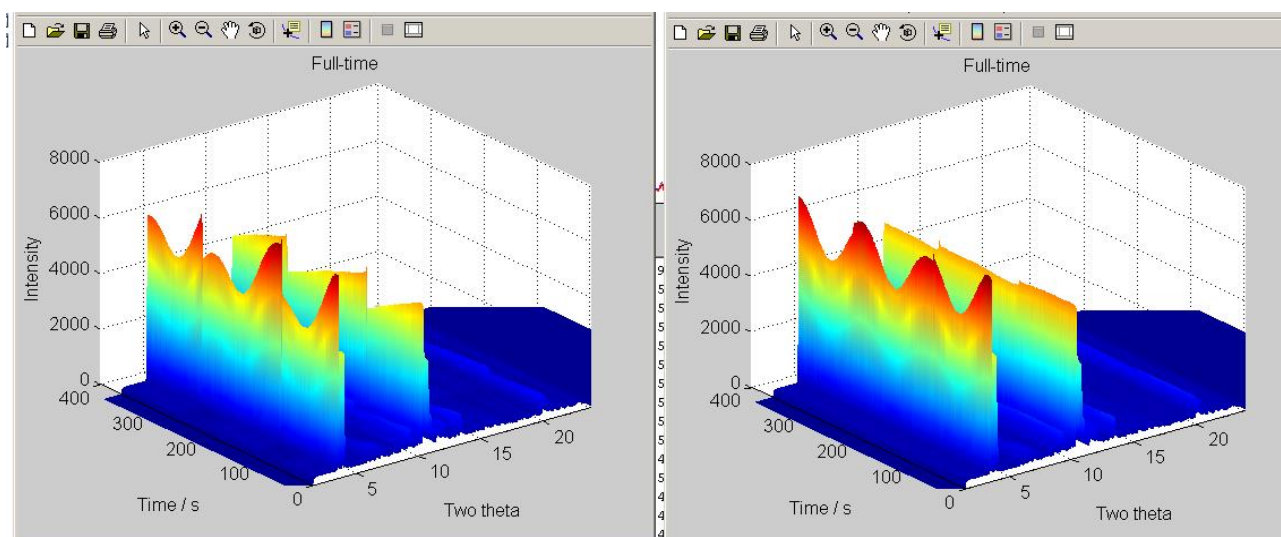


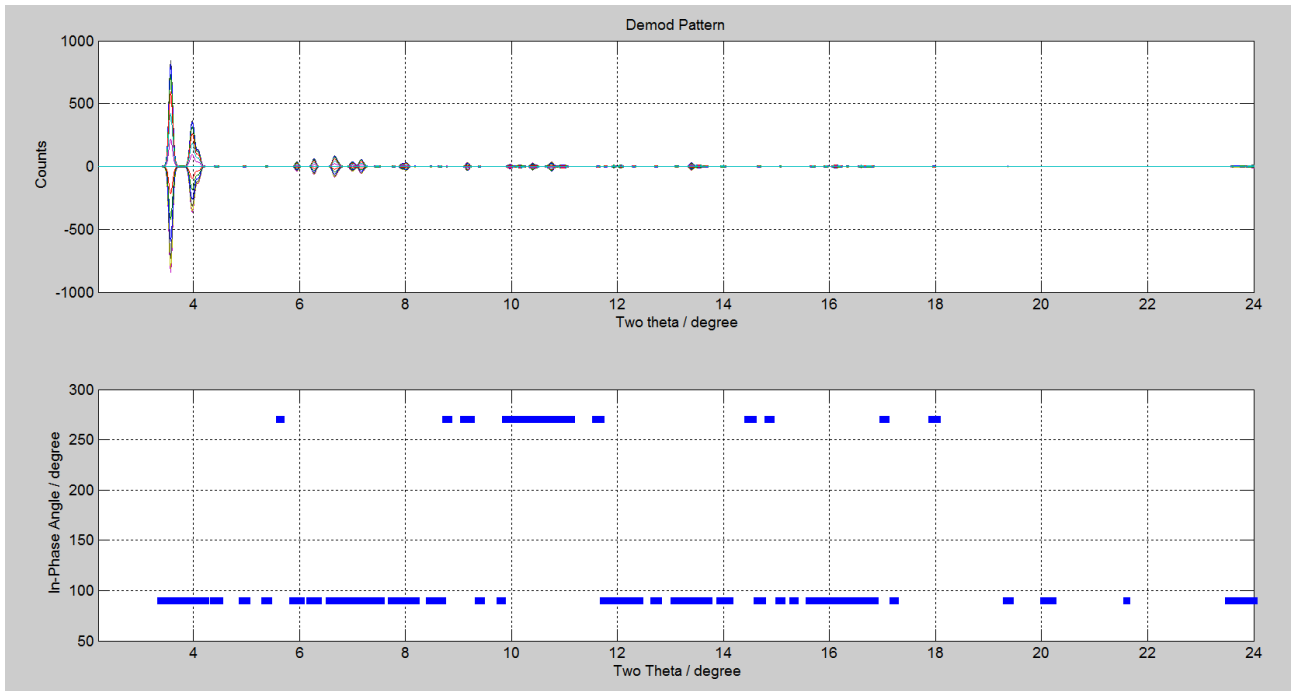
Figure SI-8: Refined occupancy of Xe in straight (black) and sinusoidal (red) channels, during T1 experiment, with highlighted the linear response region (Green ellipse) and proposed modulation in the linear range (blue line).

#### Section 4 - Pressure modulation

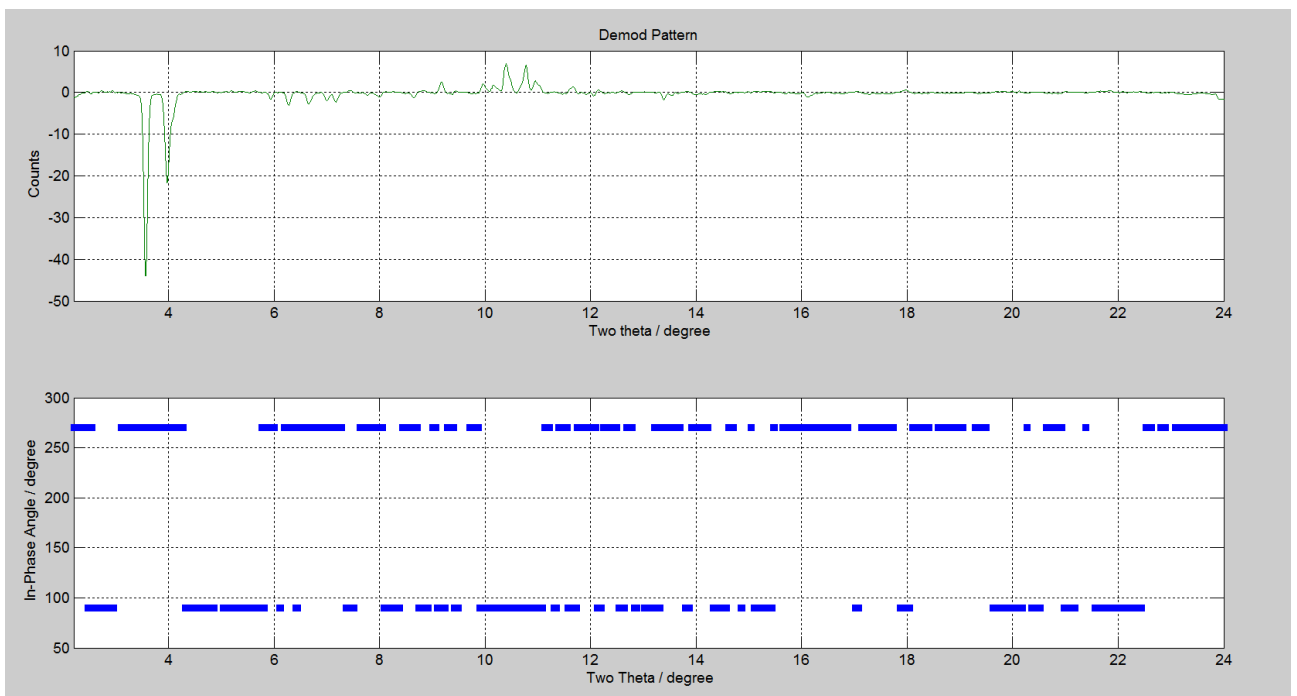
An alternative to T modulation is P modulation. By changing the pressure of the gas the amount of adsorbed gas is modified and the XRPD pattern changes accordingly (Figure SI9a). The pressure modulation at isothermal conditions, in principle reproduce the same electron density variation as in isobar temperature modulation experiments, but without (or very small) lattice variation, thus solving one of the problem of T1 experiment. MED data analysis was carried out as in simulated data. PSD detected in phase angle at 90 and 270° as expected (Figure SI-9b). In Figure S10 the constancy of peak position during the experiment can be appreciated. The same demodulation procedure was applied and the  $2\Omega$  demodulated pattern was used to solve and refine the crystal structure with EXPO software. Pressure modulation is in principle the best choice since the stimulus can be maximized without affecting lattice parameters, being the temperature constant. Obtaining a large P-induced stimulus with controlled shape is technically not easy. Moreover, the PCA analysis, despite being able to get a trend in the data by PC1, indicate that PC2 vs. PC1 plot shows no clear trend and PC2 seems to contain no information. For this reason, T modulation with small amplitude was finally chosen.



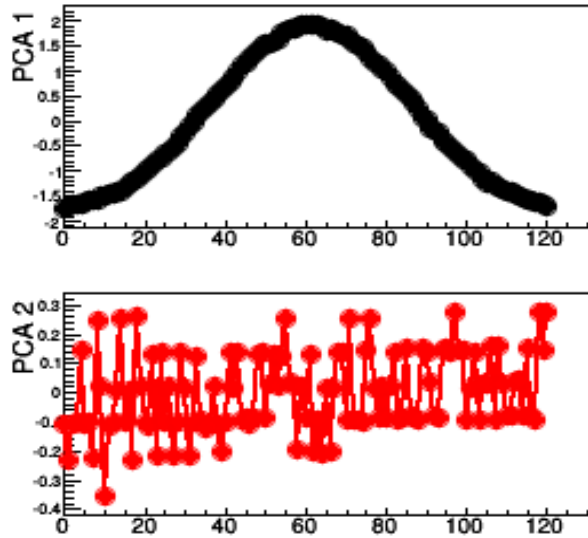
(a)



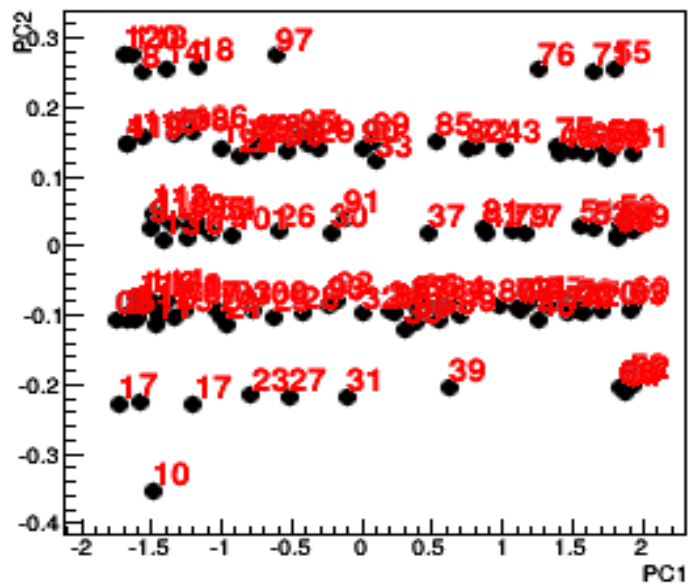
(b)



(c)

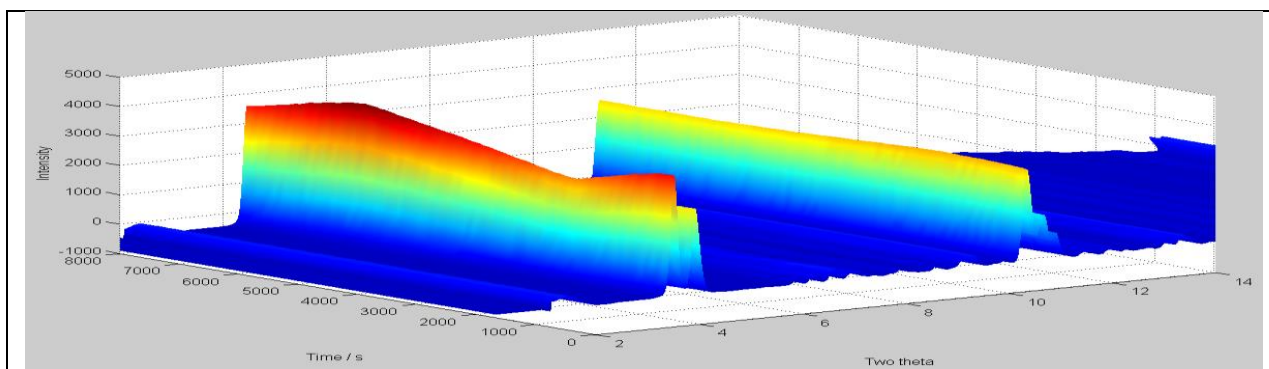


(d)

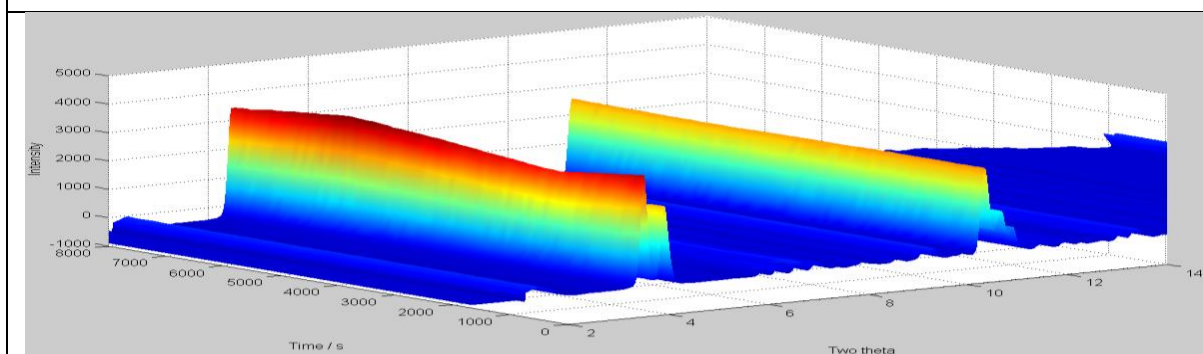


(e)

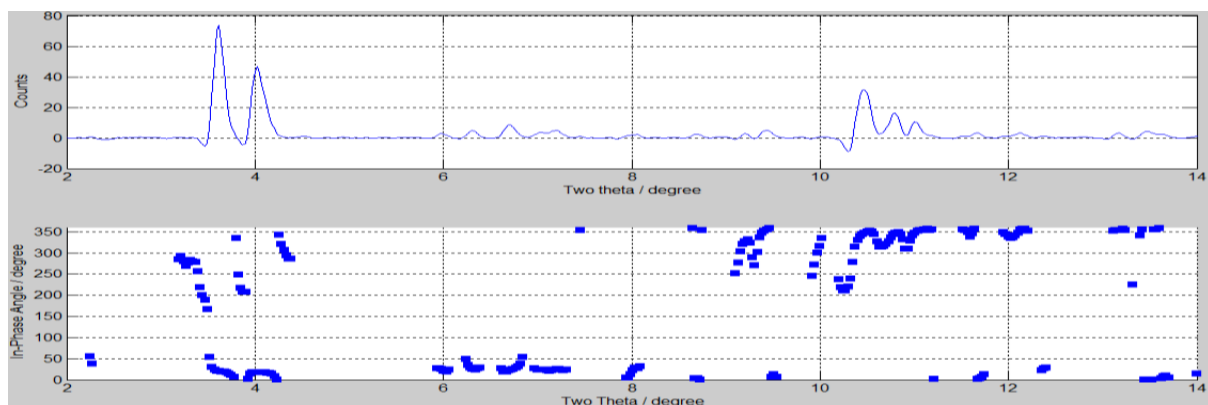
Figure SI-9: Unscaled (a-left) and scaled (a-right) pressure modulation data on the Xe-MFI system; Pattern obtained demodulating at  $2\Omega$  and PSD analysis (b); PCA analysis results for PMod data: PC1 and PC2 scores (d) and PC1 vs. C2 plot (e), clearly not showing the expected parabolic trend as T-Mod data.



(a)



(b)

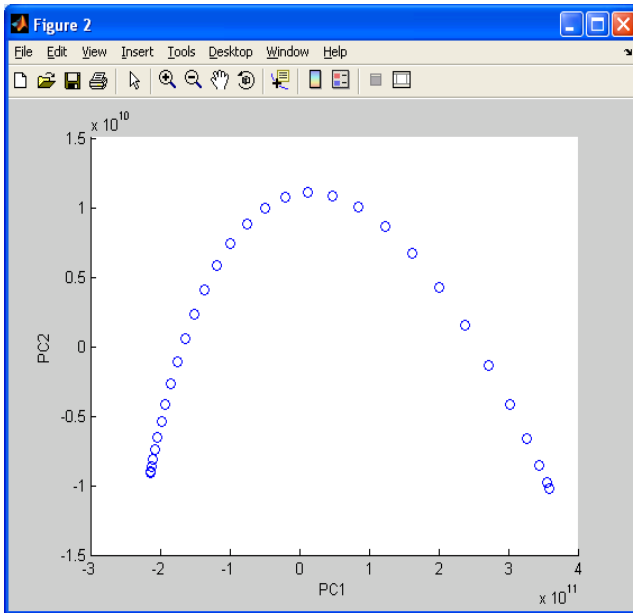


(c)

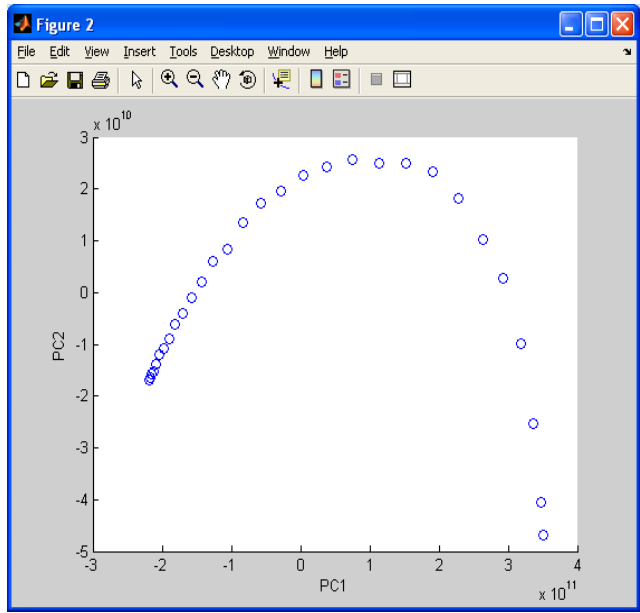
Figure SI-10: Time-domain XRPD data set for decreasing stimulus amplitudes: a) 100°K, b) 20°K, c) 10°K. Demodulation at  $2\Omega$  on real data with 20°K T window:  $2\Omega$  demodulated profile at in-phase angle=270° (d) and in-phase angle plot (e).

## Section 5 – PCA analyses

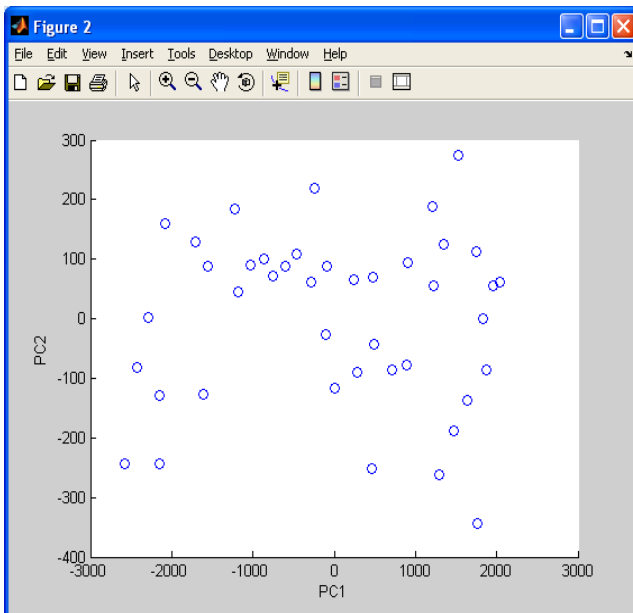
(a)



(b)



(c)



(d)

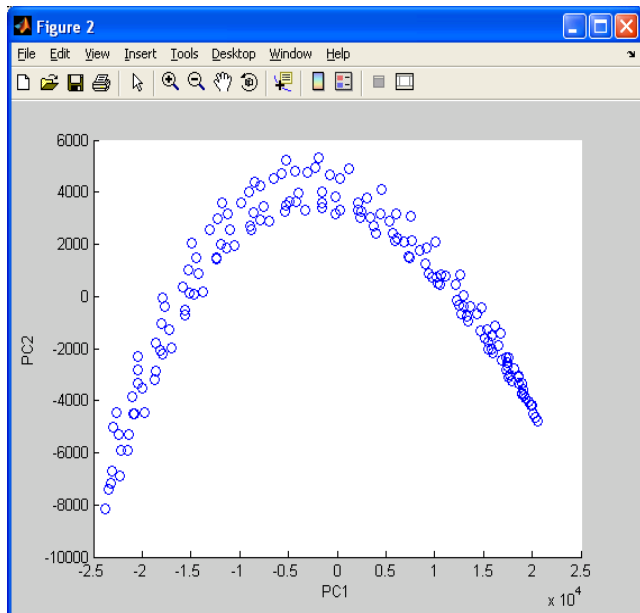


Figure SI-11: PCA analyses of simulated data (a) without and (b) with lattice variations, in comparison with T3 (c) and T6 (d) experiments.

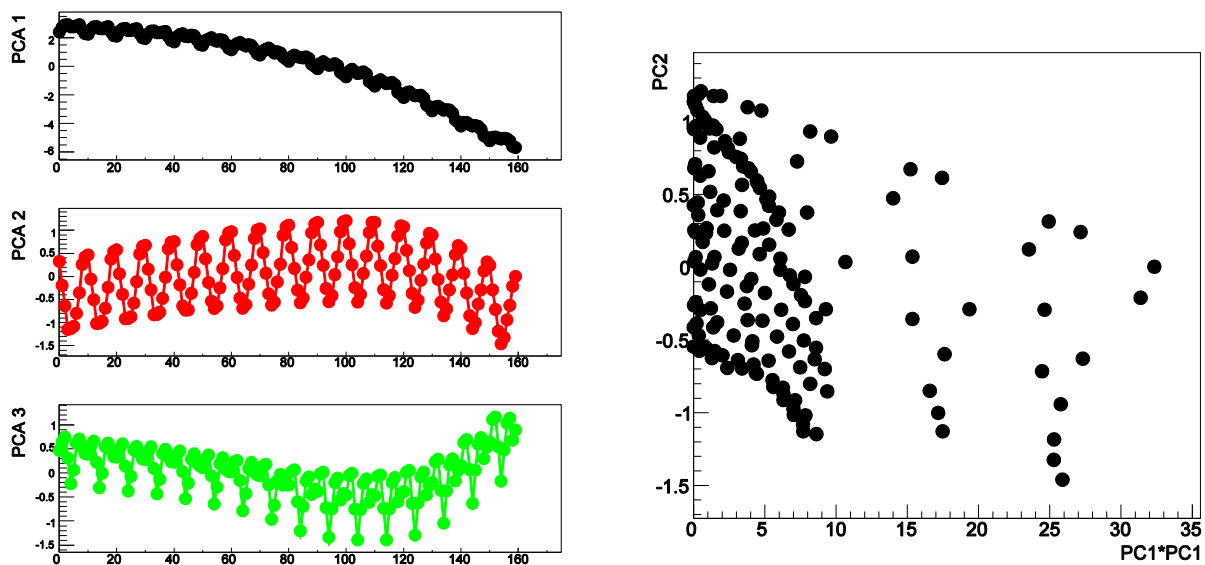


Figure SI-12: Scores of the first (PC1), second (PC2), and third (PC3) principal components for 10mbar data (T5 experiment): separate plots (a) vs. scan number, and scatter plot of PC2 versus PC1\*PC1 (b).

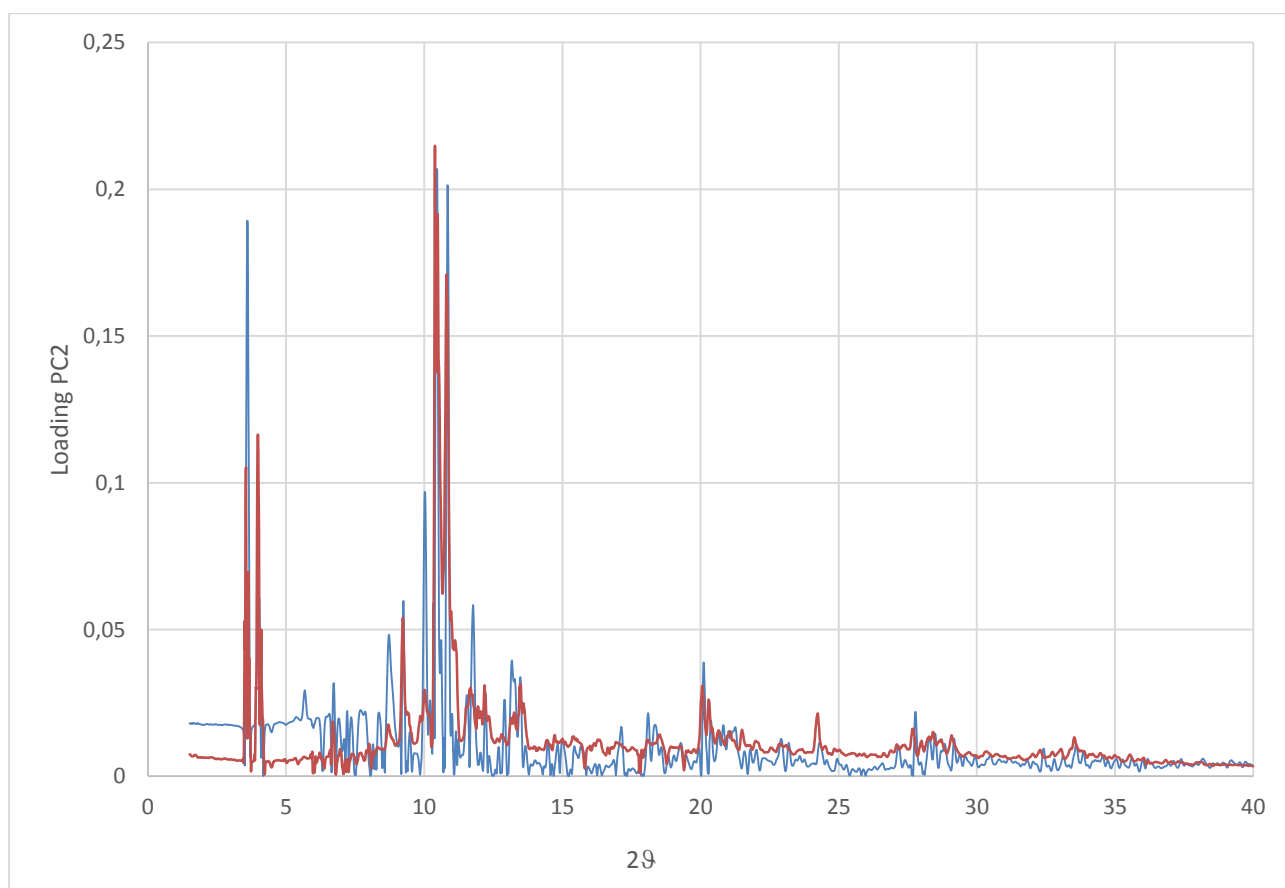
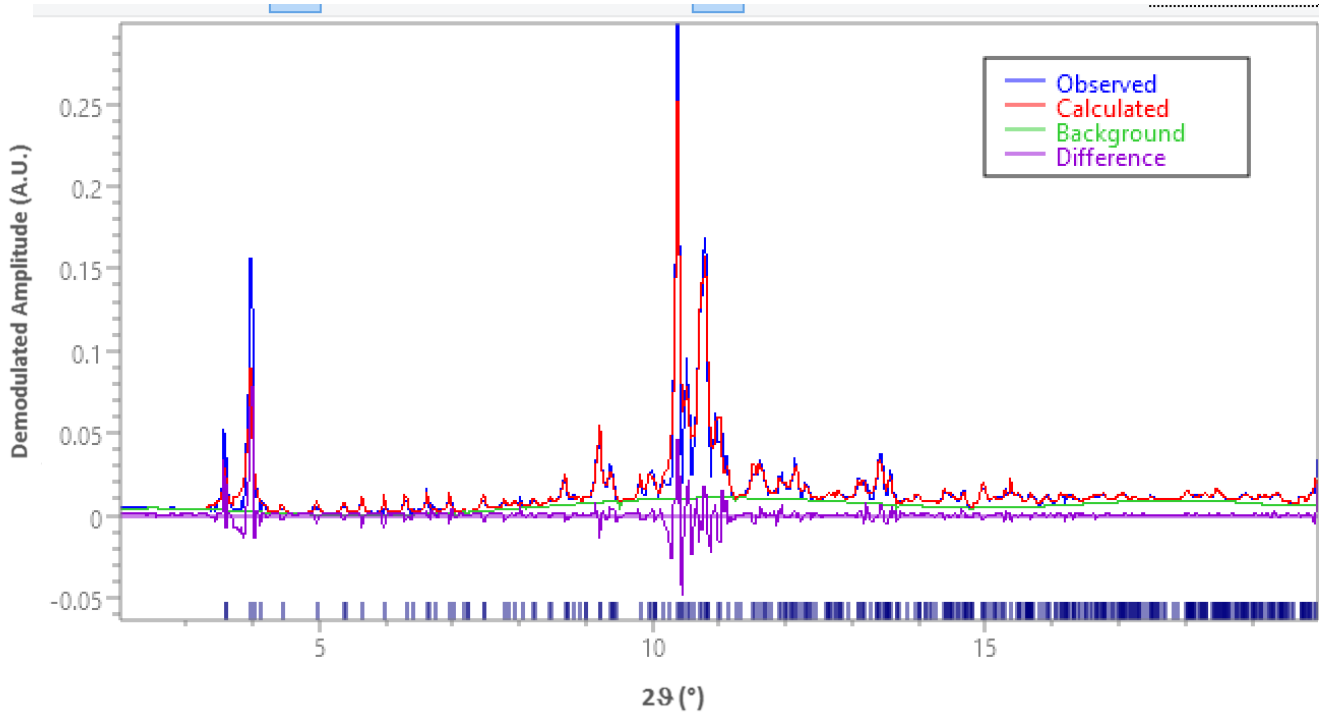
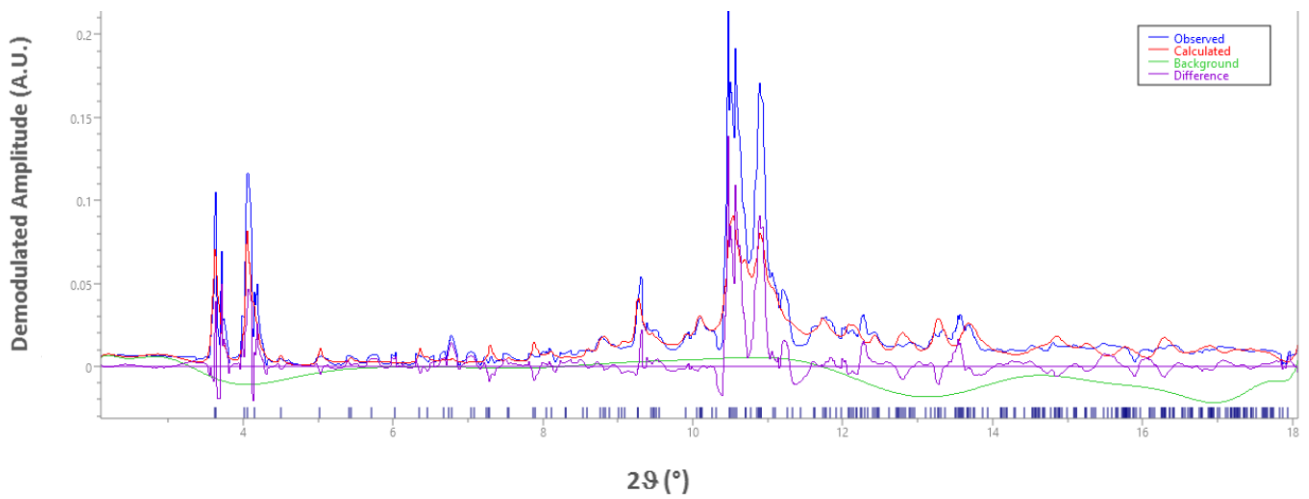


Figure SI-13: Loadings of PC2 vs. 29 for T5 (blue) and T6 (red) experiments.



(a)



(b)

Figure SI-14: Structure solution by direct methods and refinement using the EXPO software to analyze the pattern obtained demodulating the 10 mbar data by PC2: (a) peak extraction by Le Bail procedure and (b) refinement after structure solution.